

The curvature condition for self-consistent scale-free galaxies

Mir Abbas Jalali^{1,2★} and P. Tim de Zeeuw^{3†}

¹*Institute for Advanced Studies in Basic Sciences, P.O. Box 45195-159, Zanjan, IRAN*

²*Aerospace Research Institute, P.O. Box 15875-3885, Tehran, IRAN*

³*Sterrewacht Leiden, Postbus 9513, 2300 RA Leiden, The Netherlands*

18 November 2018

ABSTRACT

We modify the curvature condition for the existence of self-consistent scale-free discs, introduced by Zhao, Carollo & de Zeeuw. We survey the parameter space of the power-law discs, and show that the modified curvature condition is in harmony with the results of Schwarzschild’s numerical orbit superposition method. We study the orbital structure of the power-law discs, and find a correlation between the population of centrophobic banana orbits and the non-self-consistency index. We apply the curvature condition to other families of scale-free elongated discs and find that it rules out a large range of power-law slopes and axis ratios. We generalize the condition, and apply it, to three-dimensional scale-free axisymmetric galaxy models.

Key words: stellar dynamics – galaxies: kinematics and dynamics – galaxies: structure – methods: analytical.

1 INTRODUCTION

A key problem in stellar dynamics is the determination of the range of axis ratios and density profiles for which triaxial galaxies can be in dynamical equilibrium (see, e.g., reviews by de Zeeuw 1996; Merritt 1999). Schwarzschild (1979, 1982) attacked this issue with his linear programming method, and constructed self-consistent triaxial galaxy models with constant density cores by numerical superposition of individual stellar orbits. Similar models with separable potentials were constructed by Statler (1987) and Hunter & de Zeeuw (1992). Gerhard & Binney (1985) showed that the orbital structure in triaxial galaxies with central density cusps differs from those with cores. In particular, the box orbits are replaced by a host of minor orbit families and chaotic orbits (cf. Miralda-Escudé & Schwarzschild 1989; Lees & Schwarzschild 1992). Based on this, Gerhard (1986) already suggested that cusped triaxial galaxies would evolve towards axisymmetry. Schwarzschild (1993) showed that moderately flattened scale-free triaxial models with an r^{-2} density law could be constructed numerically, but found that these models evolved on long time scales. Similar results were obtained for non-scale-free models with steep central cusps (e.g., Merritt & Fridman 1996; Merritt 1997; Siopis 1998).

Although the general problem of the existence of self-consistent triaxial, cuspy galaxies has not been solved, valu-

able steps have been taken in the study of planar models that inherit many properties of the three-dimensional triaxial systems. Kuijken (1993, hereafter K93) applied Schwarzschild’s numerical construction method to elliptic discs with logarithmic potentials, and found that self-consistent models are ruled out for axial ratios $\lesssim 0.8$. He traced the non-existence to the properties of the chaotic orbits, in line with the three-dimensional results of Schwarzschild (1993). Sridhar & Touma (1997a, hereafter STa) introduced a class of non-axisymmetric discs whose potentials are of Stäckel form in parabolic coordinates. These discs admit an exact second integral of motion and host a continuous family of centrophobic banana orbits. Syer & Zhao (1998, hereafter SZ98) showed by numerical means that none of the STa models can be self-consistent.

Zhao, Carollo & de Zeeuw (1999, hereafter ZCZ) developed a simple analytical tool for studying the self-consistency of scale-free discs. They compared the curvature of the model density with that of individual orbits near the major axis, and showed that this leads to a necessary (but not sufficient) condition for self-consistency which can be evaluated easily. They analysed a family of elliptic discs with power-law densities for a range of slopes, and showed that the curvature condition produces results in harmony with those of K93 and SZ98. We show here that while the ZCZ approach is sound, their condition for self-consistency contains an unfortunate error, which leads to incorrect results for surface density distributions that do not fall off as $1/R$. We present the correct condition for two-dimensional

★ jalali@iasbs.ac.ir

† tim@strw.leidenuniv.nl

scale-free models, and compare the results with models constructed by means of Schwarzschild's method. This not only validates the curvature condition, but also provides insight in the proper way to apply Schwarzschild's method.

This paper is organized as follows. In §2 we introduce scale-free elongated discs, describe how self-consistent discs can be constructed with Schwarzschild's method, and re-derive and correct the curvature condition of ZCZ. In §3 we study the parameter ranges of self-consistent power-law discs, and compare the curvature results with the numerical solutions. In §4 we apply the curvature condition to three other families of elongated discs, two of which are new, and confirm the results of K93 and SZ98. We extend the curvature condition to three-dimensional scale-free axisymmetric models in §5, and apply it in §6. We summarize our conclusions in §7. We will study the triaxial case in a future paper.

2 SCALE-FREE ELONGATED DISCS

2.1 Surface-density, potential, and scaling

We consider razor-thin power-law discs with a surface density given by

$$\Sigma(R, \phi) = \Sigma_0 R^{\alpha-1} S(\phi), \quad (1)$$

and a corresponding gravitational potential

$$V(R, \phi) = \begin{cases} V_0 R^\alpha P(\phi), & \alpha \neq 0, \\ V_0 [2 \ln R + P(\phi)], & \alpha = 0, \end{cases} \quad (2)$$

where (R, ϕ) are the usual polar coordinates, and the functions $S(\phi)$ and $P(\phi)$ are related by Poisson's equation. We are interested in models which are bisymmetric, and hence restrict ourselves to $0 \leq \phi \leq \pi/2$, where $\phi = 0$ corresponds to the long axis.

Since the potential and surface density functions of our discs are scale-free, the orbits at different energies are related by simple scaling factors in length and time (e.g., Richstone 1980, hereafter R80). To find these factors, we use the equations of motion:

$$\ddot{R} - R\dot{\phi}^2 = -\frac{\partial V}{\partial R}, \quad R\ddot{\phi} + 2\dot{R}\dot{\phi} = -\frac{1}{R} \frac{\partial V}{\partial \phi}. \quad (3)$$

For a potential of the form (2) these equations are invariant under the scaling transformations

$$R = k\tilde{R}, \quad t = k^{1-\frac{\alpha}{2}} \tau, \quad (4)$$

where τ and \tilde{R} are the scaled time and radius, respectively. This means that if a star with the coordinates $[R(t), \phi(t)]$ spends a time Δt in the angular sector $\Delta\phi$, there exists another star with the coordinates $[\tilde{R}(\tau), \phi(\tau)]$ on the scaled orbit that spends the time

$$\Delta\tau = \left(\frac{R}{\tilde{R}}\right)^{\frac{\alpha}{2}-1} \Delta t, \quad (5)$$

in the same angular sector. It follows that the velocity vector (v_R, v_ϕ) scales as $(k^{\frac{\alpha}{2}} v_R, k^{\frac{\alpha}{2}} v_\phi)$.

2.2 Schwarzschild's method

The numerical construction of the self-consistent discs defined by eqs (1) and (2) is simplified by their scale-free

nature. We follow the approach of R80 and K93, and attempt to reproduce the surface density on the unit circle, $\Sigma(R=1, \phi)$. We restrict ourselves to the first quadrant and divide the unit circle into N equally spaced azimuthal cells, with surface density $\Sigma_{\text{cell}}(i) = \Sigma(R=1, \phi_i)$, $(i=1, \dots, N)$. We define $\Sigma_{\text{orb}}(i, j)$ as the mass contribution of the j th orbit ($j=1, \dots, M$) to the i th cell. The model is self-consistent if

$$\sum_{j=1}^M \Sigma_{\text{orb}}(i, j) w(j) = \Sigma_{\text{cell}}(i), \quad i = 1, \dots, N, \quad (6)$$

subject to the condition

$$w(j) \geq 0, \quad j = 1, \dots, M. \quad (7)$$

The weights $w(j)$ are a numerical representation of the phase-space distribution function that produces the surface density Σ in the potential V (cf. Schwarzschild 1979; K93).

We take $M \gg N$, so that the system of equations (6) and (7) is overdetermined. A solution of (6) subject to the constraints (7) can be found by standard linear programming (LP) methods such as the simplex method (Press et al. 1992) or the non-negative least squares (NNLS) method (Pfenniger 1984). The NNLS method is useful when kinematic constraints are included (e.g., Rix et al. 1997). We are interested only in reconstructing the surface density distribution, and we employ the simplex method through minimizing the *non-self-consistency index* Y defined in K93 as

$$Y = \frac{1}{N\bar{\Sigma}} \sum_{i=1}^N \left| \Sigma_{\text{cell}}(i) - \sum_{j=1}^M \Sigma_{\text{orb}}(i, j) w(j) \right|, \quad (8)$$

subject to the constraints $w(j) \geq 0$. The quantity Y must vanish for self-consistent discs. $\bar{\Sigma}$ is the mean surface density on the unit circle for $0 \leq \phi \leq \pi/2$.

The calculation of $\Sigma_{\text{cell}}(i)$ is straightforward through eq. (1). However, care needs to be taken with the computation of the orbital densities $\Sigma_{\text{orb}}(i, j)$. At some arbitrary time, stellar orbits do not necessarily cross the unit circle. But, some of their scaled, similar families do. The amount of mass that a star moving in the scaled orbit deposits in the azimuthal bin $\Delta\phi$ (on the unit circle) is proportional to $\Delta\tau/\Delta\phi$. According to eq. (5), this is equal to $R^{\frac{\alpha}{2}-1} \Delta t/\Delta\phi$ where we have set $\tilde{R} = 1$. Thus, having calculated the orbital density at $[R(t), \phi(t)]$, one can readily find the amount of mass contributed to the i th cell of unit circle through multiplying the obtained density by $R^{\frac{\alpha}{2}-1}$. For $\alpha = 0$, this factor is R^{-1} as noted by R80 and K93.

2.3 Curvature condition

Consider an azimuthal element of length $\Delta\phi$ on the unit circle. The surface density per unit length of this element will be $S(\phi_i)\Delta\phi$ where ϕ_i is the angular position of the centroid of the i th element. The mass contribution of the j th orbit family to the assumed azimuthal cell is proportional to $(\Delta t/T)_j R_j^{\alpha/2-1}$ where $(\Delta t/T)_j$ is the fraction of the total integration time T that a test star of orbit family j spends in the angular sector $(\phi_i, \Delta\phi)$. The model is self-consistent when (cf. eq. [6])

$$\sum_{j=1}^M w(j) \left\langle (\Delta t/T)_j R_j^{\alpha/2-1} \right\rangle = S(\phi_i) \Delta\phi, \quad i = 1, \dots, N, \quad (9)$$

where M is the number of orbits, N is the number of azimuthal cells on the unit circle, and the $w(j) \geq 0$ are weights. We have taken time averages of orbital densities (denoted by angles) for all the times when an orbit returns to the same sector. We can rewrite (9) in the form

$$\sum_{j=1}^M w(j) \left\langle \frac{(\Delta t/T)_j R_j^{\alpha/2-1}}{\Delta \phi S(\phi_i)} \right\rangle = 1, \quad i = 1, \dots, N. \quad (10)$$

In the limit, as $\Delta \phi \rightarrow 0$ so that $N \rightarrow \infty$ and we generally also need to take $M \rightarrow \infty$, one obtains

$$\sum_{j=1}^{\infty} w(j) \left\langle \frac{R_j^{\alpha/2-1}}{\phi_j S(\phi_j)} \right\rangle = 1, \quad \forall \phi_j \in \left[0, \frac{\pi}{2}\right]. \quad (11)$$

This equation is the continuous version of (6) in that the cells of configuration space are shrunk to zero size and *instantaneous* orbital densities are taken into account. The orbit families which occur in (11) can be regular or chaotic.

Eq. (11) can be expressed in terms of the angular momentum $J_j = R_j^2 \dot{\phi}_j$ as

$$\sum_{j=1}^{\infty} w(j) \langle \Gamma \rangle = 1, \quad \Gamma = \frac{1}{\|J_j\| \mu(R_j, \phi_j)}, \quad (12)$$

where we have defined

$$\mu(R_j, \phi_j) = R_j^{-\gamma} S(\phi_j), \quad \gamma = 1 + \frac{\alpha}{2}. \quad (13)$$

We assume $S(\phi)$ is smooth. Since J_j is also smooth by the equations of motion (3), we can follow ZCZ, and take the second derivative of (12) with respect to ϕ_j . This gives

$$\sum_{j=1}^{\infty} w(j) \left\langle \frac{d^2 \Gamma}{d\phi_j^2} \right\rangle = 0, \quad \forall \phi_j \in \left[0, \frac{\pi}{2}\right]. \quad (14)$$

This relation is a *necessary* condition for Γ and will be satisfied if at least some orbit families have positive $d^2 \Gamma / d\phi_j^2$ and others a negative value. If all $d^2 \Gamma / d\phi_j^2$ are either strictly positive or strictly negative, then the condition can only be satisfied by having positive as well as negative $w(j)$, so that the model is not self-consistent.

As pointed out by ZCZ, the evaluation of $d^2 \Gamma / d\phi_j^2$ is simplified considerably near the major axis of the disc. Hence, we investigate (14) at $\phi_j = 0$. We drop the subscript j of ϕ and R but keep in mind that these variables are not the same for different orbits. Following ZCZ we obtain

$$\frac{d^2 \Gamma}{d\phi^2} = \frac{\Gamma}{K_\phi} [Q_V - (1 + \gamma - \gamma\lambda)], \quad (15)$$

where

$$\lambda = [(1 + \gamma)K_R + Q_\mu K_\phi]_{\phi=0}, \quad (16)$$

and

$$K_R = \frac{\dot{R}^2}{R \frac{\partial V}{\partial R}}, \quad K_\phi = \frac{(R\dot{\phi})^2}{R \frac{\partial \mu}{\partial R}}. \quad (17)$$

The quantities Q_V and Q_μ are defined as

$$Q_V = 1 + \frac{\partial^2 V}{R \frac{\partial V}{\partial R}} \Big|_{\phi=0}, \quad Q_\mu = 1 + \frac{\partial^2 \mu}{R \frac{\partial \mu}{\partial R}} \Big|_{\phi=0}. \quad (18)$$

If $d^2 \Gamma / d\phi^2$ of eq. (15) does not have a zero, then the associated disc cannot be self-consistent.

The condition for self-consistency derived by ZCZ appears to be identical to eq. (15), but their derivation did not take into account the scaling of the orbits, which caused them to use $\mu = \mu_{ZCZ} = R^{-\gamma} S(\phi)$ and $\gamma = \gamma_{ZCZ} = 1 - \alpha$. All the formulae given in ZCZ for the second derivative of Γ are still applicable — and are indeed identical to eqs (15) to (18) — but they need to be evaluated with μ and γ given in eq. (13). The definitions (and results!) agree only when $\alpha = 0$, i.e., for discs with logarithmic potentials (i.e., flat rotation curves) such as the models studied by K93.

3 THE POWER-LAW DISCS

In order to compare the results of the curvature condition with numerically constructed discs, we now investigate a set of elongated discs with a very simple potential which makes it feasible to construct a large number of numerical models.

3.1 Potential-density pair

We take a potential of the form (2), with

$$P(\phi) = (p^2 \cos^2 \phi + \sin^2 \phi)^{\frac{\alpha}{2}}, \quad (19)$$

so that the equipotentials are similar concentric ellipses with axis ratio p . The angular dependence $S(\phi)$ of the associated surface density (1) is derived as a series expansion in Appendix A, and given in eqs (A8) and (A13). Figure 1a shows the surface density isocontours for $p = 0.2$ and $\alpha = 0.8$. They are slightly dimpled near the minor axis ($\phi = \pi/2$), where $S(\phi)$ has a minimum. The dimples become stronger as p is decreased to zero. We have numerically evaluated $S(\pi/2)$ in this limit. Figure 1b shows that the result is positive for all α , and hence demonstrates that the surface density is positive for all values of $0 \leq p \leq 1$ and $0 \leq \alpha \leq 1$.

3.2 The curvature constraint

The series expansion (A8, A13) for $S(\phi)$ can be used to show that the factor Q_μ in eq. (16) is non-negative for $0 \leq p \leq 1$ and $0 \leq \alpha \leq 1$. As a result, $0 < \lambda_{\min} \leq \lambda \leq \lambda_{\max} < \infty$. Since $\gamma = 1 + \alpha/2 > 0$, we find that the second derivative of Γ will change sign when

$$1 + \gamma - \gamma\lambda_{\max} < Q_V < 1 + \gamma - \gamma\lambda_{\min}. \quad (20)$$

This is a necessary but not sufficient condition for self-consistency. This curvature condition imposes a constraint on the curvatures of V and μ on the major axis. For $\lambda_{\min} = 0$, a non-trivial limit of (20) is obtained as

$$p > \frac{1}{\sqrt{2 + \frac{\alpha}{2}}}, \quad (21)$$

which defines the boundary curve between the allowed and forbidden zones of the parameter space (solid curve in Figure 2a). Specifically, $p > 0.707$ for $\alpha = 0$ and $p > 0.633$ when $\alpha = 1$. This corresponds to minimum axis ratios of the contours of constant surface density of 0.500 and 0.507, respectively.

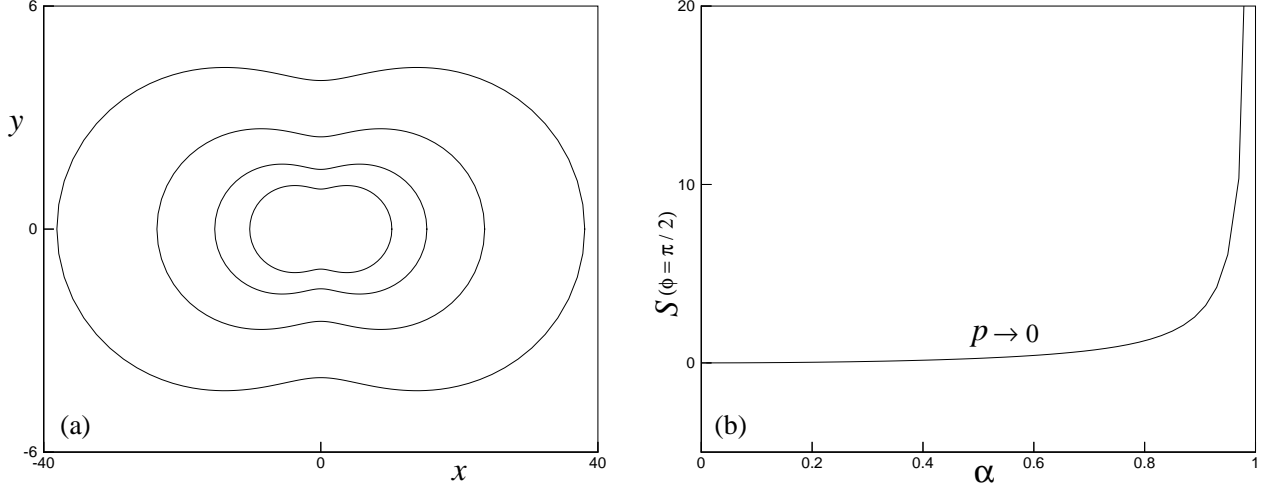


Figure 1. Panel *a* shows the surface density isocontours of the power-law disc with $p = 0.2$ and $\alpha = 0.8$. Panel *b* shows the lower bound of Σ that occurs at $\phi = \pi/2$ as $p \rightarrow 0$, as a function of α .

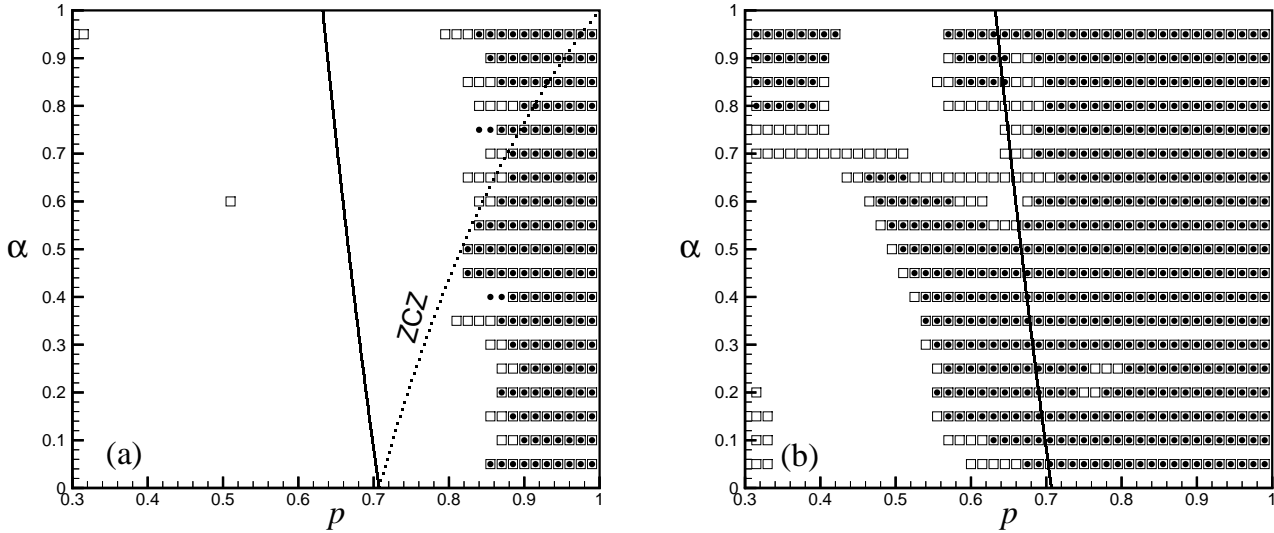


Figure 2. The (p, α) parameter space of power-law discs. For the marked points the reconstruction of the model density by Schwarzschild's numerical orbit superposition method was successful by assuming the convergence condition $\tilde{Y} < \sigma_N$, defined in equation (22) (a) Squares correspond to $N = M_2 = 45$ and filled circles correspond to $N = M_2 = 90$ (b) Squares and filled circles correspond to the pairs $(N = 45, M_2 = 180)$ and $(N = 140, M_2 = 560)$, respectively. In all cases we have set $M_1 = 80$. The solid curve is the limit (21) of the region of non-existent models provided by the curvature condition. Non-consistent models are to the left of the solid curve. The dotted line indicates the limit derived by application of the (erroneous) condition from ZCZ. The distribution of points in Panel *b* is discussed in §3.4

3.3 Numerical models

We now compare the results derived from the curvature condition with numerical models, constructed with Schwarzschild's method as outlined in §2.2. We divided the parameter space into 48 cells in the p -direction (from $p = 0.3$ to $p = 1$) and 20 cells in the α -direction (from $\alpha = 0$ to $\alpha = 1$). For each model we generated a library of M orbits containing M_1 loops (flat tubes) and M_2 orbits with zero initial velocities (along with their reflections with respect to the coordinate axes) dropped at M_2 equally spaced azimuths on the unit circle between $\phi = 0$ and $\phi = \pi/2$ (these

include fishes, bananas, pretzels, ..., cf. Miralda-Escudé & Schwarzschild 1989). We compute the surface density of the i th cell at $\phi_i = \frac{\pi}{2N}(i - \frac{1}{2})$ ($1 \leq i \leq N$), and uniformly distribute the initial positions of orbits (with zero initial velocities) on the unit circle. i.e., the j th orbit is dropped at $\phi_j = j\pi/[2(M_2 + 1)]$ where $1 \leq j \leq M_2$. In this way, initial positions of orbits will not coincide with the boundaries of cells. Our loop orbit library consists of both thin and thick orbits, which are launched on the major axis with $y(0) = \dot{x}(0) = 0$, $x(0) = 1$ and $\dot{y}(0) \geq \dot{y}_{\min} > 0$. For

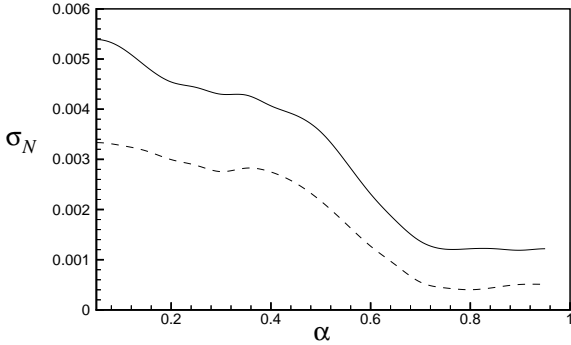


Figure 3. Variation of σ_N versus α . The solid and dashed curves correspond to $M_2 = N = 90$ and $M_2 = 4N = 560$, respectively. For each α , models having $\tilde{Y} < \sigma_N$ are accepted to be self-consistent.

$\dot{y}(0) < \dot{y}_{\min}$, the launched orbit will not belong to the 1:1 resonant island. We find \dot{y}_{\min} numerically.

In order to calculate the orbital densities, we integrated the equations of motion for up to $T = 120$ galactic years using the RK78 routine of Fehlberg (1968), which guarantees the preservation of energy with an accuracy of 10^{-12} . For a regular orbit, T should ideally be the time by which the orbit becomes dense on its invariant torus, but this may require very long integrations for near-resonant and chaotic orbits. We therefore decided to follow Cretton et al. (1999), and to fix T for all orbits to a value that is sufficiently large for the remaining variations in the orbital density not to influence the main properties of the dynamical model. Experiments showed that for $T \geq 120$ the remaining ‘noise’ in the modeling procedure is dominated by the representation of phase space through a discrete grid, and not by the properties of the individual orbit densities. We therefore chose $T = 120$ throughout.

We ran our LP code for different choices of the number N of angular cells, considered two values of the ratio M_2/N , and took $M_1 = 80$ loops in all cases. The results are illustrated in Figure 2, which shows all the points in the (p, α) -plane for which the numerical reconstruction of the model density was successful. For self-consistent discs Y should ideally become zero to within machine precision. However, our numerical computations show that for large values of p , the noise in the value of Y can have almost the same order-of-magnitude as Y itself. Thus, one needs a non-zero error threshold to pick up self-consistent models. K93 defined a threshold value for non-self-consistency based on the isotropic distribution function of axisymmetric models, even though numerical experiments showed that Y is smaller for shallow axisymmetric cusps than for steep cusps. We therefore adopted the following scheme to find a credible threshold. For each value of α , we determine the function $Y(p)$. We then filter $Y(p)$ using the Savitzky-Golay smoothing filter (Press et al. 1992) to obtain the new distribution $\tilde{Y}(p)$ from which one can calculate the noise distribution $N_Y(p) = Y(p) - \tilde{Y}(p)$. The models that we consider viable have $\tilde{Y}(p) < \sigma_N$ where σ_N is the standard deviation of the noise distribution. It is defined by

$$\sigma_N = \sqrt{\langle N_Y^2 \rangle - \langle N_Y \rangle^2}. \quad (22)$$

Figure 3 shows the variation of σ_N versus α for $M_2 = N = 90$ and $M_2 = 4N = 560$. According to this figure, shallow cusps (with $\sigma_N \approx 0.001$) have more accurate Schwarzschild models than steep ones (with $\sigma_N \approx 0.004$). We note that most of our self-consistent models have $\tilde{Y}(p) \approx 10^{-8}$, which is well within machine precision. For all successful models, noise fluctuations have been less than 1% of the global maximum of \tilde{Y} . This indicates the acceptable quality of our modeling.

Figure 2a summarizes the results of our model computations for the case $M_2 = N$, so that there is one zero-angular-momentum orbit dropped in each cell. We started our simulations with $N = 45$ (squares) and increased N until the set of self-consistent models (in the parameter space) converged (filled circles; $N = 90$). The lower bound of the allowed range of p increases as α tends to zero. Figure 2b shows the same plane, but now for the case $M_2 = 4N$. It is evident that orbits with zero initial velocities play an important role in the numerical reconstruction of the model density: by increasing M_2 relative to N , the zone of admissible parameters grows considerably, a property that was also noted by K93. We discuss the implications of this numerical result, and the difference between panels *a* and *b*, in §3.4.

In all models $\approx 90\%$ of the loop orbits have zero weight, which indicates that they are less useful in the construction of self-consistent models. This is as expected (e.g., K93) because the loop orbits of cuspy systems are universally anti-aligned with the potential and density isocontours, and they can hence only contribute part of the density (cf. de Zeeuw, Hunter & Schwarzschild 1987). As their individual orbital densities are smooth, a modest number of loops is sufficient to provide an accurate reconstruction of this part of the model density. Accordingly, the results do not depend significantly on the number M_1 of loops in the orbit catalog, and our choice $M_1 = 80$ is adequate for all cases.

3.4 Implications for Schwarzschild’s method

Figure 2a shows that the possible region for self-consistent models predicted by the curvature condition agrees well with the results of the numerically constructed models when $M_2 = N$: all of the numerically feasible models lie (well) inside the possible zone when we use $M_2 = N$. By contrast, when $M_2 = 4N$, many of the numerically acceptable solutions lie in the region forbidden by the curvature condition, even though the value of σ_N is smaller, so the condition on Y is more stringent.

The choice $M_2 > N$ is not consistent with the continuum limit expressed by eq. (11); as an azimuthal cell is shrunk to zero size, it becomes theoretically impossible to drop more than one orbit with zero initial velocity from that cell (it is still possible to launch an arbitrary number of orbits with non-zero initial velocities from the same point). In the numerical simulations with $M_2 > N$, more orbital ‘corners’ are available per cell, which brings a degree of flexibility to the LP code that in turn results in more solutions that appear acceptable. Many of these are clearly ruled out by the analytic curvature condition.

The requirement $M_2 = N$ also arises naturally in separable models, where the integral equation for the weights of the box orbits is solved analytically by assigning one box-

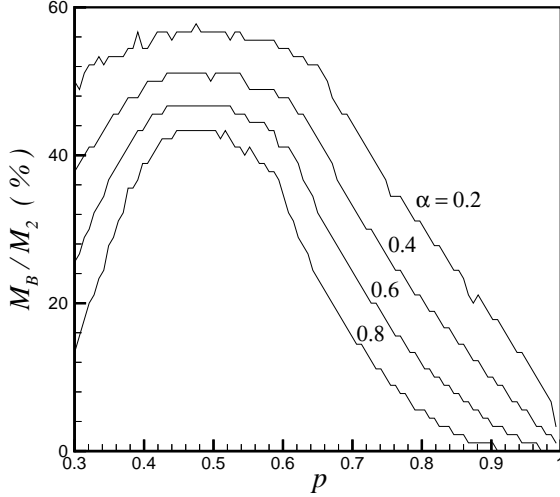


Figure 5. The variation of the relative population of banana orbits ($M_{B/2}$) versus p for several choices of α . The global maximum of $M_{B/2}$ emerges in the neighborhood of $p = 0.5$ for all values of α .

orbit corner to each cell (de Zeeuw, Hunter & Schwarzschild 1987; Statler 1987). While box orbits have one corner in the first quadrant, regular boxlets may have more, so that the rule $M_2 = N$ may count some orbits more than once (K93). We conclude that in applications of Schwarzschild's method care should be taken that the number of orbits used is matched properly to the grid of cells on which the density is reproduced.

3.5 Orbital structure

To gain a better understanding of the origin of non-self-consistency, we constructed the Poincaré maps of the orbits with zero initial velocities for several choices of α and p . We integrated the equations of motion in Cartesian coordinates, and sampled the phase space variables every time an orbit crosses the y -axis with $\dot{x} > 0$. We have used the same library of orbits as in §3.3, and dropped $M_2 = 90$ orbits from equally spaced azimuths between $\phi = 0$ and $\phi = \pi/2$. The energy $E = \frac{1}{2}v^2 + V(R, \phi)$ of all orbits was set to $E = 1$ and scaled orbits were used if needed, because orbits dropped from the unit circle do not all have the same energy. For each α , we generated the surfaces of section for two values of p : one in the forbidden zone and the other in the allowed zone of the parameter space explored by the curvature condition. The results are displayed in Figure 4. The non-self-consistent models (with $p = 0.5$) share an interesting feature: the bulk of phase space is occupied by banana orbits. By contrast, in models that are not ruled out by the curvature condition, the phase space is dominated by fishes and high-resonant orbits, while banana orbits are almost absent. This suggests that the non-self-consistency is related to the existence of centrophobic banana orbits that deposit much mass away from the major axis (as discussed also by, e.g., Pfenniger & de Zeeuw 1989; SZ98; ZCZ; Zhao 1999).

To pursue this idea further, we computed the number M_B of banana orbits, using the information in the Poincaré

maps (in the y - \dot{y} cross section; banana orbits dropped from the first quadrant never take $y > 0$). Figure 5 shows the ratio $M_{B/2} = M_B/M_2$ (in percentage) versus p for several choices of α . $M_{B/2}$ decreases when $p \rightarrow 1$ and has a maximum near $p = 0.5$. This result is not unexpected, for banana orbits emerge when the frequencies of the x - and y -oscillations are commensurate in the ratio $\omega_x/\omega_y \approx 1/2$. To first order, ω_x/ω_y equals the axial ratio p of the equipotential curves.

Figure 6 shows the computed values of the non-self-consistency index Y (for $N = M_2 = 90$ and $M_1 = 80$) versus p for the models with $\alpha = 0.8$. The best-fitted polynomial curve has a similar variation as the corresponding $M_{B/2}$ curve in Figure 5. The models with 'banana-rich' orbital structures (corresponding to $p \approx 0.5$) are *maximally* non-self-consistent. As $p \rightarrow 1$, Y decreases like $M_{B/2}$ and converges to the required accuracy of self-consistent models.

According to Figure 4, only very thin layers of chaotic orbits occur in the vicinity of hyperbolic fixed points (as also found by K93 for the logarithmic discs). Therefore, they do not seem to play an important role in the construction of the model density. This conclusion is supported by the following arguments. The orbits of a thin chaotic layer float around various resonant islands while they remain 'very close' to the outermost regular orbits (slow orbits) of these islands. It is possible to approximately generate such irregular orbits by a *random superposition* of their nearby slow orbits. Thus, in the limit when a chaotic orbit is fully mixed in the phase space, its orbital density approximately becomes equal to the density of the 'ensemble' of slow orbits. This means that a chaotic orbit enters Schwarzschild's method by adding (subtracting) a constant weight to (from) the weights of slow orbits. Our numerical computations confirm this point and reveal that our Schwarzschild models do not depend on the integration time of 'thin' chaotic orbits. The above reasoning is no longer valid for 'thick' chaotic layers, which, however, do not emerge in our models. We conclude that fishes and high-resonant orbits are the main building blocks of the self-consistent discs.

4 OTHER ELONGATED DISCS

4.1 Elliptic discs

We now consider discs with elliptic surface density distributions of the form (1), with

$$S(\phi) = (p^2 \cos^2 \phi + \sin^2 \phi)^{\frac{\alpha-1}{2}}. \quad (23)$$

The gravitational potential in the plane of the disc is of the form (2) with (e.g., Evans & de Zeeuw 1992 eq. 5.2)

$$P(\phi) = \int_0^\infty \frac{(p^2 \cos^2 \phi + \sin^2 \phi + u)^{\frac{\alpha}{2}}}{[(1+u)(p^2+u)]^{\frac{1+\alpha}{2}} u^{\frac{1}{2}}} du, \quad (24)$$

where Σ_0 and V_0 are related by $V_0 = 2\pi G \Sigma_0 p^\alpha / \alpha B(\frac{1}{2}, \frac{1-\alpha}{2})$ for $\alpha \neq 0$. When $\alpha = 0$ we have $V_0 = 2G \Sigma_0 R_F(1, p^2, 0)$, with R_F the Carlson elliptic integral of the first kind (e.g., Press et al. 1992), and

$$P(\phi) = \frac{G \Sigma_0}{V_0} \int_0^\infty \frac{\ln(p^2 \cos^2 \phi + \sin^2 \phi + u)}{[(1+u)(p^2+u)u]^{\frac{1}{2}}} du. \quad (25)$$

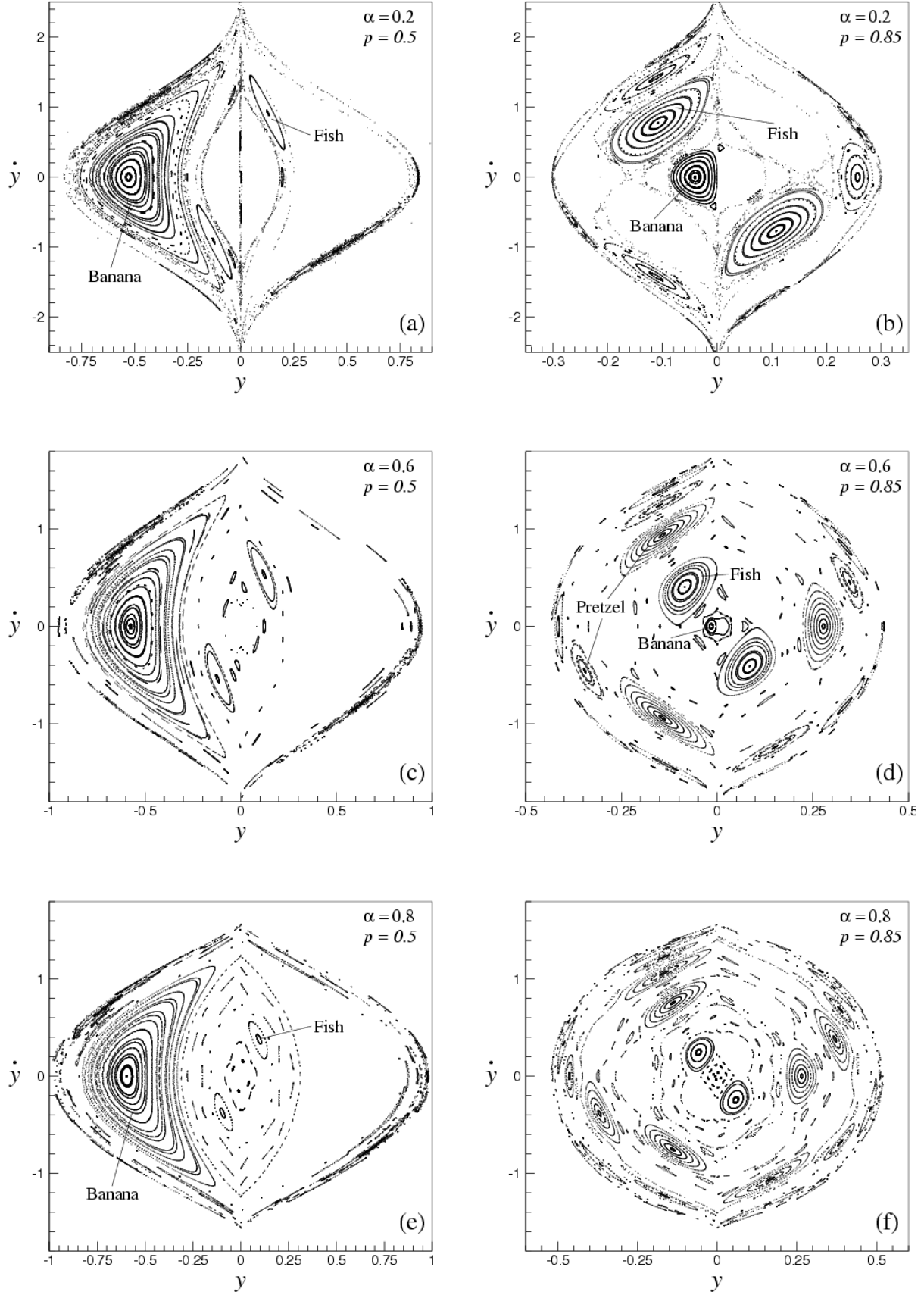


Figure 4. Poincaré maps of the orbits with zero initial velocities in the power-law discs. Orbits are dropped from equally-spaced azimuths between $\phi = 0$ and $\phi = \pi/2$. In all cases we have generated the surfaces of section for $M_2 = 90$ orbits and have set the orbital energy $E = \frac{1}{2}v^2 + V(R, \phi)$ equal to unity.

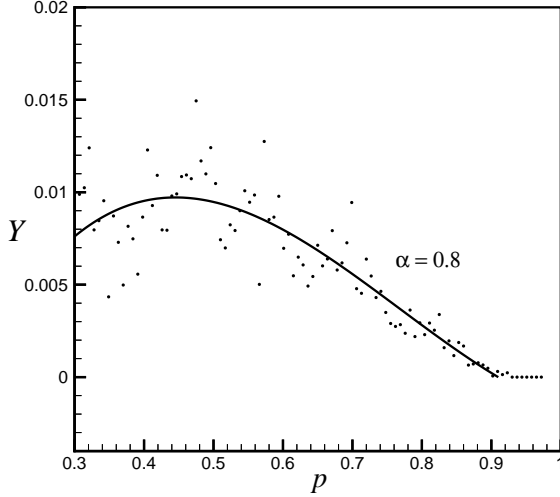


Figure 6. The variation of Y versus p for $\alpha = 0.8$, $M_1 = 80$ and $N = M_2 = 90$. The solid line is the best fitted polynomial curve to the discrete numerical data shown by dots. Similar patterns occur for the other values of α . The non-self-consistency index Y has converged to zero with an accuracy better than $\sigma_N \approx 0.001$ (for $p \gtrsim 0.9$ we arrived at $\tilde{Y} \approx 10^{-8}$).

The integrals (24) and (25) for the ϕ -dependence of the potential need to be evaluated numerically.

In order to apply the curvature condition, we evaluate Q_μ and Q_V , and obtain

$$Q_\mu = \frac{3p^2\alpha + 2(1-\alpha)}{(2+\alpha)p^2} > 0, \\ Q_V = 1 + (1-p^2) \frac{P_2(p, \alpha)}{P_1(p, \alpha)}, \quad (26)$$

where we have defined

$$P_i(p, \alpha) = \int_0^\infty u^{-\frac{1}{2}} (p^2 + u)^{\frac{1}{2}-i} (1+u)^{-\frac{1+\alpha}{2}} du, \quad (i = 1, 2). \quad (27)$$

These two integrals can be evaluated in terms of beta and hypergeometric functions (Gradshteyn & Ryzhik 1980):

$$P_i(p, \alpha) = p^{2-2i} B\left(\frac{1}{2}, \frac{2i-1+\alpha}{2}\right) {}_2F_1\left(\frac{1+\alpha}{2}, \frac{1}{2}; i + \frac{\alpha}{2}; 1-p^2\right). \quad (28)$$

They reduce to elliptic integrals when $\alpha = 0, 1$.

A necessary condition for self-consistency is obtained from (20) and (26) by assuming $\lambda_{\min} = 0$:

$$(1-p^2) \frac{P_2(p, \alpha)}{P_1(p, \alpha)} < 1 + \frac{\alpha}{2}. \quad (29)$$

The boundary curve between the allowed and forbidden zones of (29) was computed numerically and is displayed in Figure 7 (solid line). The admissible axial ratios of the logarithmic discs have an infimum of $p = 0.545$. This result agrees with the findings of K93, whose numerical studies predicted a lower bound of $p \approx 0.8$ for self-consistent models. As in the case of the power-law discs, the numerical solutions lie well inside the allowed region of parameter space.

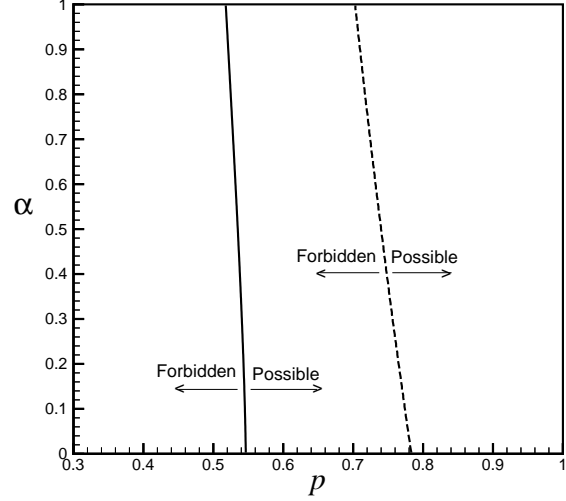


Figure 7. The parameter space of elliptic discs and projected power-law galaxies. The boundary curves between possible and non-consistent models are shown by solid and dashed lines for elliptic discs and projected power-law galaxies, respectively. Non-consistent models are to the left of boundary curves. The parameter p is the axial ratio of isodensity contours of elliptic discs. For the projected power-law galaxies, however, the parameter p is related to the axial ratio of the surface density by eqs (B5), (B6) and (B11).

4.2 Projected power-law galaxies

Projection of the density of scale-free triaxial models with potentials that are stratified on similar concentric ellipsoids (triaxial versions of the power-law galaxies of Evans 1994) provides elongated discs with surface-densities of the form (1) and associated potentials of the form (2). We have not found this potential-density pair in the literature, and give the full derivation in Appendix B. The function $S(\phi)$ is given in eq. (B10), and the function $P(\phi)$ is given in eqs (B18) and (B19). We will refer to these discs as the *projected power-law galaxies*.

On the major axis ($\phi = 0$) of projected power-law galaxies, we find

$$Q_\mu = \frac{3\alpha^2 p^4 + 6 - 6\alpha + p^2(9\alpha - 4 - 2\alpha^2)}{p^2(2+\alpha)(1+\alpha p^2)}, \\ Q_V = 1 + \frac{1-p^2}{p^2} \frac{U_2(p, \alpha)}{U_1(p, \alpha)}, \quad (30)$$

where

$$U_i(p, \alpha) = B\left(\frac{1}{2}, \frac{2i-1+\alpha}{2}\right) \times \\ \left[p^2(1+\alpha) {}_2F_1\left(\frac{3+\alpha}{2}, \frac{1}{2}; i+1+\frac{\alpha}{2}; 1-p^2\right) + \right. \\ \left. (2i-1) {}_2F_1\left(\frac{1+\alpha}{2}, \frac{1}{2}; i+1+\frac{\alpha}{2}; 1-p^2\right) \right], \quad (31)$$

with $i = 1, 2$. One can easily verify that $Q_\mu > 0$ for all values of $|\alpha| \leq 1$ and $0 \leq p \leq 1$. Therefore, the necessary condition for self-consistency becomes

$$\frac{(1-p^2)}{p^2} \frac{U_2(p, \alpha)}{U_1(p, \alpha)} < 1 + \frac{\alpha}{2}. \quad (32)$$

The boundary curve between the allowed and forbidden

zones of inequality (32) is displayed in Figure 7 (dashed line). In comparison with the power-law discs, the self-consistency of a larger fraction of the parameter space is ruled out for the projected power-law galaxies.

4.3 Sridhar–Touma discs

The separable discs introduced by STa have

$$P(\phi) = [(1 + \sin \phi)^{1+\alpha} + (1 - \sin \phi)^{1+\alpha}], \quad (33)$$

where $0 < \alpha < 1$. The associated density function $S(\phi)$ is given in eq. (4) of STa as a one-dimensional integral. From (33) we obtain $Q_V = 2 + \alpha$ and $Q_\mu > 0$. Upon substituting these results into (20) we arrive at the requirement

$$2 + \alpha < 2 + \frac{\alpha}{2}, \quad (34)$$

which shows that self-consistent models are ruled out for all admissible values of α . This is identical to the conclusion drawn by SZ98, based on another method. The non-self-consistency of STa models can also be interpreted by our arguments of §3.5. All STa models, which have the fixed axial ratio $p = 0.5$ of equipotential curves (for all values of the cusp slope), are non-self-consistent because they host only a continuous family of centrophobic banana orbits.

5 SCALE-FREE AXISYMMETRIC GALAXIES

We now extend the curvature condition to scale-free axisymmetric models, in which the orbits can be described as two-dimensional motion in the meridional plane.

5.1 Potential-density pairs

Consider spherical polar coordinates (r, θ, ϕ) where r is the radial distance from the origin, θ is the colatitude and ϕ is the azimuthal angle. We denote the momenta conjugate to (r, θ, ϕ) by (p_r, p_θ, p_ϕ) . In axisymmetric systems, the component $p_\phi \equiv L_z$ of the angular momentum vector parallel to the symmetry axis is a conserved quantity. Furthermore, the variable ϕ does not explicitly occur in the potential-density pairs, which take the following forms in scale-free models

$$\begin{aligned} V &= \begin{cases} V_0 \text{sgn}(\alpha) r^\alpha P(\theta), & \alpha \neq 0, \\ V_0 [2 \ln r + P(\theta)], & \alpha = 0, \end{cases} \\ \rho &= \rho_0 r^{\alpha-2} S(\theta), \quad \alpha < 2. \end{aligned} \quad (35)$$

5.2 Derivation of the curvature condition

The curvature condition (15) can be extended to three-dimensional axisymmetric models if we define Γ as

$$\Gamma = \frac{1}{\|L_j\| \mu(r_j, \theta_j)}, \quad (36)$$

where

$$L = \left(p_\theta^2 + \frac{L_z^2}{\sin^2 \theta} \right)^{1/2}, \quad (37)$$

is the modulus of the angular momentum and (cf. eq. [13])

$$\mu(r_j, \theta_j) = r_j^{-\gamma} S(\theta_j), \quad \gamma = 1 + \frac{\alpha}{2}. \quad (38)$$

The subscript j refers to the j th orbit family. The scaling properties of planar discs given in (4) will be valid for three-dimensional models if we replace R with r . The smoothness condition for Γ becomes

$$\sum_{j=1}^{\infty} w(j) \left\langle \frac{d^2 \Gamma}{d\theta_j^2} \right\rangle = 0, \quad \forall \theta_j \in \left[0, \frac{\pi}{2} \right], \quad (39)$$

where $\theta = \pi/2$ corresponds to the equatorial plane. This is identical to equation (14), but now applies to axisymmetric systems. As before, we drop the subscript j and write

$$\begin{aligned} \frac{1}{\Gamma} \frac{d^2 \Gamma}{d\theta^2} &= -\frac{1}{L} \frac{d^2 L}{d\theta^2} - \frac{1}{\mu} \frac{d^2 \mu}{d\theta^2} + 2 \frac{dL}{L d\theta} \frac{d\mu}{\mu d\theta} \\ &\quad + 2 \left(\frac{1}{L} \frac{dL}{d\theta} \right)^2 + 2 \left(\frac{1}{\mu} \frac{d\mu}{d\theta} \right)^2. \end{aligned} \quad (40)$$

We confine ourselves to the region near the equatorial plane. This simplifies the expressions considerably. For the models having reflection symmetry with respect to the equatorial plane, we have $\partial \mu / \partial \theta = \partial V / \partial \theta = 0$ at $\theta = \pi/2$.

The first and second derivatives of L and μ with respect to θ can be obtained using the equations of motion

$$\dot{r} = p_r, \quad \ddot{r} = \dot{p}_r = -\frac{\partial V}{\partial r} + \frac{p_\theta^2}{r^3} + \frac{L_z^2}{r^3 \sin^2 \theta}, \quad (41)$$

$$\dot{\theta} = \frac{p_\theta}{r^2}, \quad \dot{p}_\theta = -\frac{\partial V}{\partial \theta} + \frac{L_z^2 \cos \theta}{r^2 \sin^3 \theta}. \quad (42)$$

At $\theta = \pi/2$, eq. (42) implies $\dot{p}_\theta = dp_\theta/d\theta \approx 0$, which leads to $r\ddot{\theta} + 2\dot{r}\dot{\theta} \approx 0$ near the equatorial plane. Furthermore, from (37) we find that $dL/d\theta$ vanishes at $\theta = \pi/2$. By using (42) we find

$$\left[-\frac{1}{L} \frac{d^2 L}{d\theta^2} \right]_{\theta=\pi/2} = \left[\frac{1}{1 + \frac{L_z^2}{p_\theta^2}} \left(\frac{1}{r^2 \theta^2} \frac{\partial^2 V}{\partial \theta^2} \right) \right]_{\theta=\pi/2}. \quad (43)$$

The derivatives of μ with respect to θ can be expressed in terms of $dr/d\theta$ and $d^2 r/d\theta^2$, which we evaluate by means of the equations of motion and the condition $r\ddot{\theta} + 2\dot{r}\dot{\theta} \approx 0$ which is valid near $\theta = \pi/2$.

Combining all terms in expression (40), and carrying out some algebraic manipulations, then leads to

$$\left[\frac{d^2 \Gamma}{d\theta^2} \right]_{\theta=\pi/2} = \left\{ \frac{\Gamma}{K_\theta} [\kappa Q_V - (\kappa + \gamma - \gamma\lambda)] \right\}_{\theta=\pi/2}, \quad (44)$$

where

$$\lambda = Q_\mu K_\theta + (1 + \gamma) K_r + K_\phi, \quad (45)$$

with

$$K_r = \frac{\dot{r}^2}{r \frac{\partial V}{\partial r}}, \quad K_\theta = \frac{(r\dot{\theta})^2}{r \frac{\partial V}{\partial \theta}}, \quad K_\phi = \frac{1}{r \frac{\partial V}{\partial r}} \frac{L_z^2}{r^2}, \quad (46)$$

and

$$\kappa = \left(1 + \frac{K_\phi}{K_\theta} \right)^{-1}, \quad (47)$$

and the quantities Q_V and Q_μ are defined by

$$Q_V = 1 + \frac{\partial^2 V}{r \frac{\partial V}{\partial r}} \Big|_{\theta=\pi/2}, \quad Q_\mu = 1 + \frac{\partial^2 \mu}{r \frac{\partial \mu}{\partial r}} \Big|_{\theta=\pi/2}. \quad (48)$$

These expressions resemble those for the elongated disc case, but contain the additional parameter κ .

A necessary condition for self-consistency follows from (44) as

$$\kappa + \gamma - \gamma\lambda_{\max} < \kappa Q_V < \kappa + \gamma - \gamma\lambda_{\min}. \quad (49)$$

The greatest upper bound of (49) corresponds to $\lambda_{\min} = 0$. Therefore, a non-trivial condition for self-consistency is

$$Q_V < 1 + \frac{\gamma}{\kappa}. \quad (50)$$

6 APPLICATIONS

We now apply the curvature criterion to three families of scale-free axisymmetric galaxy models.

6.1 The power-law galaxies

The power-law galaxies of Evans (1993, 1994) have

$$S(\theta) = \begin{cases} \alpha [m_1^2(\theta)]^{\frac{\alpha-4}{2}} [2q^2 - m_1^2(\theta) + \alpha m_2^2(\theta)], & \alpha \neq 0, \\ 2 [m_1^2(\theta)]^{-2} [2q^2 - m_1^2(\theta)], & \alpha = 0, \end{cases} \quad (51)$$

and

$$P(\theta) = \begin{cases} [m_1^2(\theta)]^{\alpha/2}, & \alpha \neq 0, \\ \ln m_1^2(\theta), & \alpha = 0, \end{cases} \quad (52)$$

where $V_0 = 4\pi G\rho_0$ and we have defined $m_k^2(\theta) = q^{2k} \sin^2 \theta + \cos^2 \theta$. The density function ρ is positive for $q^2 > (1-\alpha)/2$. The parameter β introduced in Evans (1994) is equivalent to $-\alpha$.

From (52) we find $Q_V = 1/q^2$. Therefore, the condition (50) reduces to

$$q^2 > \frac{2\kappa}{2\kappa + 2 + \alpha}. \quad (53)$$

This shows that the self-consistency of the power-law models is not ruled out near the equatorial plane.

The above inequality has an interesting interpretation: since the quantity κ is a dynamical property of orbit families, as it involves not only the potential but also L_z , we can investigate whether an orbit family is useful for the self-consistency of a given model. For example, $\kappa = 1$ corresponds to orbits confined completely to a meridional plane ($L_z = 0$), and therefore, we can rule out self-consistent models with

$$q < \frac{1}{\sqrt{2 + \frac{\alpha}{2}}}, \quad (54)$$

using only the meridional orbits. This is the same result obtained for the power-law discs in §3.2. As κ tends to zero, the amplitude of vertical motions decreases and more flattened models are supported. In the limit, the models with $q = 0$ become self-consistent for $\kappa = 0$. Thus, equatorial orbits are essential building blocks of highly flattened models in general and limiting circular discs in particular.

6.2 Scale-free spheroids

Scale-free galaxy models with spheroidal density isocontours have widely been used in galactic dynamics (Qian et al. 1995, hereafter Q95). In this case

$$S(\theta) = [m_1^2(\theta)]^{\frac{\alpha}{2}-1}, \quad (55)$$

and

$$P(\theta) = \begin{cases} \int_0^\infty \frac{(q^2 \sin^2 \theta + \cos^2 \theta + u)^{\frac{\alpha}{2}} du}{(1+u)^{1+\frac{\alpha}{2}} (q^2+u)^{\frac{1+\alpha}{2}}}, & \alpha \neq 0, \\ \frac{\pi G \rho_0}{q V_0} \int_0^\infty \frac{\ln(q^2 \sin^2 \theta + \cos^2 \theta + u) du}{(1+u)(q^2+u)^{\frac{1}{2}}}, & \alpha = 0, \end{cases} \quad (56)$$

where $V_0 = 2\pi G\rho_0 q^{\alpha-1}/\alpha$ for $\alpha \neq 0$ and $V_0 = 2\pi G\rho_0 R_F(1, 1, q^2)/q$ for $\alpha = 0$. R_F is the Carlson elliptic integral of the first kind.

Oblate models have $0 < q < 1$ and prolate models have $q > 1$. We restrict ourselves to the range $-1 < \alpha < 1$.

The curvature parameter Q_V (in the equatorial plane $\theta = \pi/2$) is

$$Q_V = 1 + (1 - q^2) \frac{V_2(q, \alpha)}{V_1(q, \alpha)}, \quad (57)$$

where

$$V_i(q, \alpha) = q^{2-2i} B\left(1, i + \frac{\alpha-1}{2}\right) {}_2F_1\left(1 + \frac{\alpha}{2}, 1; i + \frac{1+\alpha}{2}; 1 - q^2\right), \quad (58)$$

for oblate models and

$$V_i(q, \alpha) = q^{2-2i} B\left(1, i + \frac{\alpha-1}{2}\right) {}_2F_1\left(\frac{2i-1}{2}, 1; i + \frac{1+\alpha}{2}; 1 - \frac{1}{q^2}\right), \quad (59)$$

for prolate ones. By inserting expression (57) in the condition (50), and noting that $\gamma = 1 + \frac{\alpha}{2}$, we obtain the necessary condition for self-consistency as

$$\frac{(1 - q^2) V_2(q, \alpha)}{V_1(q, \alpha)} < \frac{1}{\kappa} \left(1 + \frac{\alpha}{2}\right). \quad (60)$$

Numerical computations show that the left-hand side of (60) is positive for oblate models and negative for prolate ones. So, the condition (60) is fulfilled by the proper choices of $0 < \kappa < 1$, and we cannot rule out any models.

6.3 Oblate Sridhar–Touma models

The oblate mass models described by Sridhar & Touma (1997b, hereafter STb) are the extensions of the flat STa models to three-dimensional space. These axisymmetric, cuspy models are integrable and admit an exact third integral of motion. We have shown elsewhere (Jalali & de Zeeuw 2001) that exact two- and three-integral distribution functions can be constructed for these models. It is useful to determine what the curvature condition gives.

The STb models have

$$S(\theta) = (\alpha - \cos \theta)(1 + \cos \theta)^\alpha + (\alpha + \cos \theta)(1 - \cos \theta)^\alpha, \quad (61)$$

and

$$P(\theta) = (1 + \cos \theta)^{1+\alpha} + (1 - \cos \theta)^{1+\alpha}, \quad (62)$$

where $1 < \alpha < 2$. It follows that Q_V is given by $Q_V = 1 + \alpha$, which upon substitution in (50) yields the condition

$$\alpha < \frac{1}{\kappa} \left(1 + \frac{\alpha}{2}\right). \quad (63)$$

This is satisfied for $\alpha < 2$ and all possible orbits corresponding to $0 < \kappa < 1$, as expected based on the results of Jalali & de Zeeuw (2001). The phase space of STb models consists of a continuous family of reflected banana orbits all of which are useful for the construction of self-consistent equilibria.

7 DISCUSSION

Lynden-Bell (1962) showed that the distribution function of a stellar system depends on the phase-space coordinates through the isolating integrals of motion. However, such integrals of motion are not available for most physical models. In fact, there are few mathematical models of galaxies that have separable potentials. Finding the integrals of motion is a formidable task for non-integrable systems. The existence of $f(E, L_z)$ distribution functions for axisymmetric models (with E the orbital energy and L_z the angular momentum parallel to the symmetry axis) has helped galactic dynamicists to develop more realistic galaxy models and extract their observable properties (e.g., Q95). But, in non-axisymmetric systems, only E is conserved, and we have to adopt other construction methods. Schwarzschild's (1979) paper was a major step in this way. His elegant numerical method allowed astronomers to attack the self-consistency problem of galaxy models from a different point of view, by constructing the coarse-grained distribution functions as weighted sums of the densities of individual stellar orbits without explicit knowledge of non-classical integrals of motion.

Schwarzschild's method does not require restrictions on the shape of the model or the functional form of the potential, and can be applied to non-integrable models as well as integrable ones. The only drawback is the cost of the numerical computations, especially when the number of cells in the configuration space is large and the orbit library is rich. Although supercomputers can handle massive calculations, a quick mathematical tool has always been attractive. ZCZ developed one such tool, which is a simple mathematical test for self-consistency, and applied it to scale-free elongated discs. The idea derives from the fact that by increasing the number of orbits and cells in Schwarzschild's method, one can obtain a limiting analytical expression for the conditions of dynamical equilibrium. The smoothness condition for the quantity Γ is such an interpretation of Schwarzschild's method. The curvature condition says that if the discrete numerical equations (subject to the positivity constraints on the weight functions) is solvable, a relation between the curvatures of the potential and density functions must be satisfied. This results in a necessary condition for equilibrium. It takes a particularly simple form near the major axis of the model where the surface density isocontours are strongly curved, and the reconstruction of the density profile is most difficult, as it requires boxlets and chaotic orbits. We have corrected an error in the ZCZ derivation of the curvature condition, and also extended it to motion in axisymmetric potentials.

The curvature condition is necessary but not sufficient, so we can use it to detect non-consistency, but cannot prove self-consistency. We can only state that in the allowed region of the parameter space, explored by the curvature condition, scale-free self-consistent models may be found. Our exper-

iments on the power-law discs show that the results of the curvature condition (applied to the major axis of elongated discs) do indeed provide a boundary inside which the numerical solutions lie, and they furthermore have highlighted the need to be careful with the choice of the catalog of zero-angular momentum orbits when applying Schwarzschild's method.

Our results reveal a correlation between the non-self-consistency index Y and the relative population of banana orbits $M_{B/2}$ (as suspected in many of the earlier studies quoted). Maximally non-self-consistent power-law discs (for $p \approx 0.5$) have banana-rich orbital structures independent of the value of α . We speculate that this property is shared by all razor-thin discs whose potential functions allow for the existence of 1:2 resonant orbits, and conclude that it is of interest to search for more elongated discs without bananas (Jalali 1999; Sridhar & Touma 1999).

In the case of three-dimensional axisymmetric models, we have employed our test near the equatorial plane where the circular orbits and equatorial rosettes overwhelm the effect of other orbit families. The existence of the L_z integral provides an extra quantity κ that can be controlled to satisfy the necessary condition of self-consistency. This dynamical property of orbit families does not occur in the study of planar non-axisymmetric systems and is not expected to appear in triaxial systems. It is known that $f(E, L_z)$ distribution functions cannot be constructed for most prolate models (an upper bound exists for the allowed axial ratios of prolate models versus the cusp slope, e.g., Evans 1994, Q95), but the curvature condition does not reject the self-consistency of prolate galaxies. This is not a shortcoming, for the curvature condition is necessary but not sufficient.

Our next goal is to extend the curvature condition to scale-free triaxial galaxies. The step to non-scale-free models remains as another challenging problem.

8 ACKNOWLEDGMENTS

The authors thank HongSheng Zhao for useful discussions and Nicolas Cretton for providing the RK78 routine. Comments by the referee C. Siopis helped us to improve the presentation in §3. MAJ thanks the hospitality of Sterrewacht Leiden where this work was begun. NOVA, the Netherlands Research School for Astronomy, provided partial funding for the visit.

REFERENCES

- Andrews L.C., Shivamoggi B.K., 1986, *Integral Transforms* (McMillan Publ), p. 35
- Binney J.J., 1981, *MNRAS*, 196, 455
- Cretton N., de Zeeuw P.T., van der Marel R.P., Rix H.-W., 1999, *ApJS*, 124, 383
- Evans N.W., 1993, *MNRAS*, 260, 191
- Evans N.W., 1994, *MNRAS*, 267, 333
- Evans N.W., de Zeeuw P.T., 1992, *MNRAS*, 257, 152
- Evans N.W., Carollo C.M., de Zeeuw P.T., 2000, *MNRAS*, 318, 1131
- Fehlberg E., 1968, *NASA TR* 287
- Gerhard O.E., 1986, *MNRAS*, 219, 373
- Gerhard O.E., Binney J.J., 1985, *MNRAS*, 216, 467

- Gradshteyn I.S., Ryzhik I.M., 1980, Table of Integrals, Series and Products, 4th edition, Academic Press, New York
- Hunter C., de Zeeuw P.T., 1992, ApJ, 389, 79
- Jalali M.A., 1999, MNRAS, 310, 97
- Jalali M.A., de Zeeuw P.T., 2001, MNRAS, 328, 511
- Kuijken K., 1993, ApJ, 409, 68 (K93)
- Lees J.F., Schwarzschild M., 1992, ApJ, 384, 491
- Lynden-Bell D., 1962, MNRAS, 124, 1
- Merritt D., 1997, ApJ, 486, 102
- Merritt D., 1999, PASP, 111, 129
- Merritt D., Fridman T., 1996, ApJ, 460, 136
- Miralda-Escudé J., Schwarzschild M., 1989, ApJ, 339, 752
- Morse P.M., Feshbach H., 1953, Methods of Theoretical Physics (McGraw-Hill), p. 837
- Pfenniger D., 1984, A&A, 141, 171
- Pfenniger D., de Zeeuw P.T., 1989, in Dynamics of Dense Stellar Systems, ed. D.R. Merritt (Cambridge Univ. Press), 81
- Press W.H., Teukolsky S.A., Vetterling W.T., Flannery B.P., 1992, Numerical Recipes, Cambridge Univ. Press
- Qian E.E., de Zeeuw P.T., van der Marel R.P., Hunter C., 1995, MNRAS, 274, 602 (Q95)
- Richstone D.O., 1980, ApJ, 238, 103 (R80)
- Rix H.-W., de Zeeuw P.T., Cretton N., van der Marel R.P., Carollo C.M., 1997, ApJ, 488, 702
- Schwarzschild M., 1979, ApJ, 232, 236
- Schwarzschild M., 1982, ApJ, 263, 599
- Schwarzschild M., 1993, ApJ, 409, 563
- Siopis, C., 1998, PhD Thesis, Univ. of Florida
- Sridhar S., Touma J., 1997a, MNRAS, 287, L1 (STa)
- Sridhar S., Touma J., 1997b, MNRAS, 292, 657 (STb)
- Sridhar S., Touma J., 1999, MNRAS, 303, 483
- Stark A.A., 1977, ApJ, 213, 368
- Statler T.S., 1987, ApJ, 321, 113
- Syer D., Tremaine S.D., 1996, MNRAS, 281, 925
- Syer D., Zhao H.S., 1998, MNRAS, 296, 407 (SZ98)
- de Zeeuw P.T., 1996, in Gravitational Dynamics, eds O. Lahav, E. Terlevich, R.J. Terlevich (Cambridge Univ. Press), 1
- de Zeeuw P.T., Franx M., 1989, ApJ, 343, 617
- de Zeeuw P.T., Hunter C., Schwarzschild M., 1987, ApJ, 317, 607
- de Zeeuw P.T., Pfenniger D., 1988, MNRAS, 235, 949
- Zhao H.S., 1999, MNRAS, 309, 636
- Zhao H.S., Carollo C.M., de Zeeuw P.T., 1999, MNRAS, 304, 457 (ZCZ)

APPENDIX A: THE SURFACE DENSITY OF THE POWER-LAW DISCS

We derive the surface density associated with the disc potential

$$V(R, \phi) = V_0 R^\alpha (p^2 \cos^2 \phi + \sin^2 \phi)^{\alpha/2}, \quad 0 < \alpha < 1, \quad (\text{A1})$$

with $0 < p < 1$. We introduce $\epsilon = 1 - p$ and rewrite the disc potential in the form

$$V = V_0 R^\alpha (1 - 2t \cos \phi + t^2)^{\alpha/2}, \quad (\text{A2})$$

where $t = \epsilon \cos \phi$ with $|t| < 1$ (we exclude the case $\epsilon = 1$ from our calculations). The ϕ -dependence of V can now be expanded in terms of Gegenbauer polynomials as (see eq. [8.930] in Gradshteyn & Ryzhik 1980)

$$V = V_0 R^\alpha \sum_{n=0}^{\infty} C_n^\lambda(\cos \phi) t^n, \quad (\text{A3})$$

where $\lambda = -\alpha/2$ and

$$C_n^\lambda(\cos \phi) = \sum_{k=0}^n \frac{\Gamma(\lambda + k) \Gamma(\lambda + n - k)}{k! (n - k)! [\Gamma(\lambda)]^2} \cos(2k - n)\phi. \quad (\text{A4})$$

We now expand the term t^n in a Fourier series, and write

$$\cos^n \phi = \sum_{m=0}^n \beta_m^{(n)} \cos m\phi, \quad (\text{A5})$$

where $\beta_m^{(n)} = 0$ when $n - m$ is odd and

$$\beta_m^{(n)} = \begin{cases} \frac{1}{2^{n-1}} \binom{n-m}{2}, & m \neq 0, \\ \frac{1}{2^n} \binom{n}{n/2}, & m = 0, \end{cases} \quad (\text{A6})$$

when $n - m$ is even. Using expressions (A4) and (A5), the potential function becomes

$$V = \frac{V_0 R^\alpha}{2} \sum_{n=0}^{\infty} \sum_{m=0}^n \sum_{k=0}^n \epsilon^n \beta_m^{(n)} \frac{\Gamma(\lambda + k) \Gamma(\lambda + n - k)}{k! (n - k)! [\Gamma(\lambda)]^2} \times [\cos(2k - n + m)\phi + \cos(2k - n - m)\phi]. \quad (\text{A7})$$

Now, we use eqs (A1) and (A5) of Syer & Tremaine (1996, hereafter ST96) to find the surface densities corresponding to single Fourier modes and superpose the results. Interestingly, the surface density becomes

$$\Sigma = \frac{-V_0 R^{\alpha-1}}{2\pi G} \sum_{n=0}^{\infty} \sum_{m=0}^n \sum_{k=0}^n \epsilon^n \beta_m^{(n)} \frac{\Gamma(\lambda + k) \Gamma(\lambda + n - k)}{k! (n - k)! [\Gamma(\lambda)]^2} \times [F(s_1) \cos s_1 \phi + F(s_2) \cos s_2 \phi], \quad (\text{A8})$$

where

$$F(s_i) = \frac{\Gamma(s_i/2 + \alpha/2 + 1) \Gamma(s_i/2 - \alpha/2 + 1/2)}{\Gamma(s_i/2 + \alpha/2 + 1/2) \Gamma(s_i/2 - \alpha/2)},$$

$$s_1 = 2k - n + m,$$

$$s_2 = 2k - n - m. \quad (\text{A9})$$

The minus sign in front of (A8) is cancelled once the Gamma functions are evaluated.

The case $\alpha = 0$, which corresponds to logarithmic potentials, is special and needs a different treatment. In this case we have

$$V(R, \phi) = V_0 [2 \ln R + \ln(1 - 2t \cos \phi + t^2)]. \quad (\text{A10})$$

The second term in (A10) can be expanded as the series (Gradshteyn & Ryzhik 1980, eq. [1.514])

$$\ln(1 - 2t \cos \phi + t^2) = -2 \sum_{n=1}^{\infty} \frac{\cos n\phi}{n} t^n, \quad (\text{A11})$$

which after the substitution $t = \epsilon \cos \phi$ and using $\ln(1 - z) = -\sum_{n=1}^{\infty} z^n/n$, gives the potential as

$$V = V_0 \left\{ 2 \ln \left(1 - \frac{\epsilon}{2} \right) + 2 \ln R - \sum_{n=1}^{\infty} \frac{\epsilon^n}{2^{n-1} n} \cos 2n\phi - \sum_{n=1}^{\infty} \sum_{m=0}^{n-1} \frac{\epsilon^n \beta_m^{(n)}}{n} [\cos(n+m)\phi + \cos(n-m)\phi] \right\}. \quad (\text{A12})$$

By dropping the constant term in V and using eq. (A5) of ST96, we obtain the surface density as

$$\Sigma(R, \phi) = \frac{V_0}{\pi G R} \left[1 + \sum_{n=1}^{\infty} \frac{\epsilon^n}{2^{n-1}} \cos k\phi + \sum_{n=1}^{\infty} \sum_{m=0}^{n-1} \frac{\epsilon^n \beta_m^{(n)}}{2n} (i \cos i\phi + j \cos j\phi) \right], \quad (\text{A13})$$

with $k = 2n$, $i = n + m$ and $j = n - m$.

A simple representation for Σ is

$$\Sigma(R, \phi) = \frac{1}{R} \left(a_0 + \sum_{\ell=1}^{\infty} a_{\ell} \cos \ell\phi \right), \quad a_0 = \frac{V_0}{\pi G}, \quad (\text{A14})$$

where the Fourier coefficients a_{ℓ} ($\ell \geq 1$) are given by

$$a_{\ell} = \frac{V_0}{\pi G} \sum_{n=1}^{\infty} \left[\frac{\epsilon^n \delta_{k,\ell}}{2^{n-1}} + \sum_{m=0}^{n-1} \frac{\epsilon^n \beta_m^{(n)}}{2n} (i \delta_{i,\ell} + j \delta_{j,\ell}) \right], \quad (\text{A15})$$

with

$$\delta_{r,s} = \begin{cases} 1, & r = s, \\ 0, & r \neq s. \end{cases} \quad (\text{A16})$$

From the definition of $\beta_m^{(n)}$, we conclude that $a_{\ell} = 0$ when ℓ is odd. Using the rule $\Gamma(z+1) = z\Gamma(z)$ and eq. (A5) of ST96, the potential function can be regenerated from (A14) as

$$V = 2\pi G a_0 \ln R - 2\pi G \sum_{\text{even } \ell > 0}^{\infty} \frac{a_{\ell}}{\ell} \cos \ell\phi, \quad (\text{A17})$$

which is identical to the result obtained by K93 for aligned discs (the coefficients a_{ℓ} of K93 are computed for an elliptic disc with flat rotation curve).

APPENDIX B: THE PROJECTED POWER-LAW GALAXIES

We compute the projected surface density of the scale-free triaxial power-law models, for arbitrary direction of viewing, and show that the resulting surface density has a simple form. We consider it as the surface density of an elongated scale-free disc, and show that the gravitational potential in this disc can be evaluated explicitly. This then defines a new family of elongated discs which we call the projected power-law galaxies.

B1 Scale-free triaxial power-law models

Consider scale-free triaxial power-law models with gravitational potential

$$V(x, y, z) = \begin{cases} \frac{1}{2} v_c^2 \ln \left(x^2 + \frac{y^2}{p^2} + \frac{z^2}{q^2} \right), & \alpha = 0, \\ \frac{1}{\alpha} v_c^2 \left(x^2 + \frac{y^2}{p^2} + \frac{z^2}{q^2} \right)^{\alpha/2}, & 0 < \alpha < 1. \end{cases} \quad (\text{B1})$$

The associated density distribution is (Binney 1981; de Zeeuw & Pfenniger 1988)

$$\rho(x, y, z) = \frac{v_c^2}{4\pi G} \frac{Ax^2 + By^2 + Cz^2}{(x^2 + p^{-2}y^2 + q^{-2}z^2)^{2-\frac{\alpha}{2}}}, \quad (\text{B2})$$

with

$$\begin{aligned} A &= \frac{1}{p^2} + \frac{1}{q^2} - 1 + \alpha, \\ B &= \frac{1}{p^2} \left(1 - \frac{1-\alpha}{p^2} + \frac{1}{q^2} \right), \\ C &= \frac{1}{q^2} \left(1 + \frac{1}{p^2} - \frac{1-\alpha}{q^2} \right). \end{aligned} \quad (\text{B3})$$

This is the triaxial generalization of the axisymmetric power-law galaxies of Evans (1993, 1994). The surfaces of constant density are not ellipsoidal and become dimpled near the short axis when q is small (e.g., Evans, Carollo & de Zeeuw 2000). The density distribution (B2) is non-negative as long as $q^2 + p^2 q^2 - (1-\alpha)p^2 \geq 0$. This is a non-trivial constraint except in the limit $\alpha \rightarrow 1$.

B2 Projected surface density

Now observe the density (B2) from an arbitrary direction defined by the standard spherical polar coordinates (θ, ϕ) . Define a coordinate system (x'', y'', z'') such that the z'' axis lies along the line-of-sight and the x'' axis lies in the (x, y) -plane. The relations between (x, y, z) and (x'', y'', z'') are given in, e.g., de Zeeuw & Franx (1989). Direct integration shows that $\Sigma(x'', y'')$ is an elementary function, given by

$$\Sigma(x'', y'') = \frac{v_c^2}{4\pi G} \frac{pqB \left(\frac{1}{2}, \frac{1}{2} - \frac{\alpha}{2} \right)}{\left(c_1 c_3 - \frac{1}{4} c_2^2 \right)^{1+\frac{\alpha}{2}}} \times \frac{a_1 x''^2 - a_2 x'' y'' + a_3 y''^2}{(c_1 x''^2 - c_2 x'' y'' + c_3 y''^2)^{\frac{3}{2}-\frac{\alpha}{2}}}, \quad (\text{B4})$$

where

$$\begin{aligned} c_1 &= \sin^2 \phi + p^2 \cos^2 \phi, \\ c_2 &= 2(1 - p^2) \sin \phi \cos \phi \cos \theta, \\ c_3 &= \cos^2 \phi \cos^2 \theta + p^2 \sin^2 \phi \cos^2 \theta + q^2 \sin^2 \theta, \end{aligned} \quad (\text{B5})$$

and

$$\begin{aligned} a_1 &= c_1 c_3 - \frac{1}{4} c_2^2 + \alpha \left(c_1^2 + \frac{1}{4} c_2^2 \right), \\ a_2 &= \alpha c_2 (c_1 + c_3), \\ a_3 &= c_1 c_3 - \frac{1}{4} c_2^2 + \alpha \left(c_3^2 + \frac{1}{4} c_2^2 \right). \end{aligned} \quad (\text{B6})$$

The surface density is scale-free, and has biaxial symmetry.

Now transform to polar coordinates (R, Φ'') defined by $(x'', y'') = (R \cos \Phi'', R \sin \Phi'')$. Then the major axis of Σ lies at position angle $\Phi'' = \Phi^*$, with

$$\tan 2\Phi^* = \frac{c_2}{c_3 - c_1} = \frac{a_2}{a_3 - a_1}. \quad (\text{B7})$$

This is the expected result: as the potential is stratified on ellipsoids, its projection is stratified on similar concentric ellipses at the fixed position angle Φ^* (Stark 1977), and this is then also the position angle of the projected surface density.

When we rotate the coordinate system to (R, Φ) where $\Phi = \Phi'' - \Phi^*$, we obtain

$$\Sigma(R, \Phi) = \Sigma_0 R^{\alpha-1} S(\bar{\mu}), \quad (\text{B8})$$

where

$$\Sigma_0 = \frac{v_c^2}{4\pi G} \frac{2^{\frac{3}{2}+\frac{\alpha}{2}} B \left(\frac{1}{2}, \frac{1-\alpha}{2} \right) pqP}{(c_1 + c_3 - \Delta)^{\frac{3}{2}+\frac{\alpha}{2}}}, \quad (\text{B9})$$

and

$$S(\bar{\mu}) = \frac{(1-\alpha)P^2 + \alpha(1+P^2)\bar{\mu}}{\bar{\mu}^{\frac{3}{2}-\frac{\alpha}{2}}}. \quad (\text{B10})$$

with

$$P^2 = \frac{c_1 + c_3 - \Delta}{c_1 + c_3 + \Delta}, \quad \Delta = \sqrt{(c_1 - c_3)^2 + c_2^2} \quad (\text{B11})$$

and we have defined the abbreviation $\bar{\mu} = P^2 \cos^2 \Phi + \sin^2 \Phi$ which will be useful below.

Unlike ρ , the projected surface density Σ is everywhere positive. The angular dependence of the projected surface density has the same form for *all* directions of observation, but the value of P is a function of the intrinsic axis ratios p and q and the viewing angles θ and ϕ . The isophotes are slightly oval. An example is shown in Figure 4 of Evans, Carollo & de Zeeuw (2000). The axis ratio P' of the surface density, defined as $S(x', 0) = S(0, P'x')$ is given by

$$P' = \frac{P}{[(1+\alpha)(1+\alpha p^2)]^{1/(1-\alpha)}} \quad (\text{B12})$$

which reduces to P when $\alpha = 0$. When the model is observed down the z -axis, we have ϕ is arbitrary, $\theta = 0$, and $P = p$.

B3 Potential in the disc

Now consider surface densities of the form (B4) with $S(\bar{\mu})$ given by (B10) where without loss of generality we take $P = p$ and $\Phi = \phi$ (see above). We take Σ_0 given, but note that (B9) could be used to relate it to a three-dimensional model.

The potential $V(x, y)$ in the plane of the disc can be evaluated with the formalism developed by Evans & de Zeeuw (1992, §5). They decompose a given biaxial scale-free disc into a weighted integral of constituent discs with elliptic surface densities of different axis ratios. As the potential of the constituent discs is known from classical theory, their weighted integral provides the potential of our given disc. Specifically, if we can find the function $w(\tau)$ such that

$$S(\bar{\mu}) = \int_0^\infty \frac{w(\tau) d\tau}{(\tau + \bar{\mu})^{\frac{1}{2}-\frac{\alpha}{2}}}, \quad (\text{B13})$$

then the potential in the disc is

$$V(R, \bar{\mu}) = \frac{2\pi G \Sigma_0 R^\alpha}{\alpha B\left(\frac{1}{2}, \frac{1}{2} - \frac{\alpha}{2}\right)} \int_0^\infty w(\tau) [(1+\tau)(p^2+\tau)]^{\frac{\alpha}{2}} d\tau \\ \times \int_0^\infty \frac{(u+\bar{\mu}+\tau)^{\frac{\alpha}{2}} du}{u^{1/2} [(u+p^2+\tau)(u+1+\tau)]^{\frac{1}{2}+\frac{\alpha}{2}}}, \quad (\text{B14})$$

when $\alpha \neq 0$, and

$$V(R, \bar{\mu}) = A \ln R + B(\bar{\mu}), \quad (\text{B15})$$

with

$$A = 4G \Sigma_0 \int_0^\infty w(\tau) R_F(\tau+1, \tau+p^2, 0) d\tau, \\ B(\bar{\mu}) = G \Sigma_0 \int_0^\infty \int_0^\infty \frac{\ln(u+\bar{\mu}+\tau) w(\tau) d\tau du}{u^{1/2} (u+p^2+\tau)^{1/2} (u+1+\tau)^{\frac{1}{2}}}, \quad (\text{B16})$$

when $\alpha = 0$. Here R_F is the Carlson elliptic integral of the first kind (e.g., Press et al. 1992), and we have corrected some typographical errors in expressions (5.10) and (5.11) of Evans & de Zeeuw (1992).

For the specific case with $S(\bar{\mu})$ given in eq. (B10), the integral equation (B13) can be solved to give (with $P = p$)

$$w(\tau) = \alpha(1+p^2)\delta(\tau) + 2p^2\delta'(\tau), \quad (\text{B17})$$

where $\delta(\tau)$ is the Dirac delta function and $\delta'(\tau)$ is its derivative (see, e.g., Morse & Feshbach 1953, p. 837 or Andrews & Shivamoggi 1986, p. 35). The delta functions reduce the integrals (B16) and (B14) to single integrations. We find

$$V(R, \bar{\mu}) = \frac{2\pi G \Sigma_0 p^{2+\alpha} R^\alpha}{\alpha B\left(\frac{1}{2}, \frac{1}{2} - \frac{\alpha}{2}\right)} \int_0^\infty \frac{(u+\bar{\mu})^{\frac{\alpha}{2}} du}{u^{\frac{1}{2}} [(1+u)(p^2+u)]^{\frac{1}{2}+\frac{\alpha}{2}}} \\ \times \left(\frac{1+\alpha}{p^2+u} + \frac{1+\alpha}{1+u} - \frac{\alpha}{u+\bar{\mu}} \right), \quad (\text{B18})$$

for $\alpha \neq 0$. For $\alpha = 0$ the coefficients A and B in eq. (B15) are given by

$$A = \frac{4}{3} p^2 G \Sigma_0 [R_D(0, 1, p^2) + R_D(0, p^2, 1)], \\ B(\bar{\mu}) = 2p^2 G \Sigma_0 \int_0^\infty \left(\frac{1}{u+p^2} + \frac{1}{u+1} \right) \frac{\ln(u+\bar{\mu}) du}{\sqrt{u(u+p^2)(u+1)}} \\ - \frac{4}{3} p^2 G \Sigma_0 R_J(0, p^2, 1, \bar{\mu}), \quad (\text{B19})$$

where R_D and R_J are the Carlson elliptic integrals of the second and third kind, available in the standard numerical libraries.